ЖУРНАЛ СТРУКТУРНОЙ ХИМИИ

2017. Том 58, № 4 *Май – июнь* *С. 692 – 701*

UDC 541.6:543.422:547.12

A DFT STUDY ON THE STRUCTURAL AND ELECTRONIC PROPERTIES OF SMALL TOXIC GASES ON B- AND Al-DOPED C_{20} FULLERENE

F. Molani[1], M. Askari[2]

[1]*Young Researchers and Elite Club, Sanadaj Branch, Islamic Azad University, Sanandaj, Iran*
E-mail: f.molani@gmail.com
[2]*Department of Chemistry, Faculty of Science, Sanandaj Branch, Islamic Azad University, Sanandaj, Iran*

Received October, 14, 2015 *Revised — December, 9, 2016*

The structural and electronic properties of semiconducting BC_{19} and AlC_{19} heterofullerenes as adsorbents for toxic small gas molecules (H_2S and SO_2) are determined by DFT. Structural parameters, energy gaps, natural population analysis, partial density of state, dipole moments, and vibrational frequencies were extracted. The adsorption process and sensitivity to the gases are increased by doping with B or Al. The results show that AlC_{19} is the most sensitive structure. The good sensing of AlC_{19} is related to high charge transfer upon gas adsorption. Adsorption of the H_2S on the BC_{19} has negligible effects on the electronic properties, to be categorized as ″harmless adsorption″. H_2S is weakly adsorbed on BC_{19} and AlC_{19}. The H_2S and SO_2 molecules act as electron donating and electron withdrawing molecules, respectively. Notably, the adsorption processes are highly exothermic. In general, BC_{19} is more reactive than C_{20} and AlC_{19} is the most reactive cage. This provides a theoretical basis to fabricate B- and Al-doped C_{20}-based gas sensors.

DOI: 10.15372/JSC20170403

K e y w o r d s: heterofullerene, electronic structure, toxic gas sensing, DFT.

INTRODUCTION

According to Euler′s theorem, fullerenes are molecules that made up of exactly 12 pentagons and a differing number of hexagons [1]. In 1985, C_{60} as one of the most famous fullerenes with 12 pentagons and 20 hexagons was discovered [2]. The fullerenes are promising candidates for basic elements in nanoscale systems. The C_{20} molecule with only 12 pentagons is the smallest member of the fullerene family [3]. After detection of the C_{20} in different phases [3—5], many theoretical and experimental studies on this smallest carbon cluster have been performed [6—17]. The C_{20} fullerenes with different symmetries have very close energies and similar properties [9, 15, 17]. In addition, thermal stability and strong reactivity of C_{20} have been confirmed [16, 17]. Despite the many studies on the C_{20}, small effort has been made to assess the C_{20} fullerene as a potential agent for adsorption of the small gases, even though many studies have been performed on potential applications of nanostructures for gas adsorption [16, 18—30]. One of the main challenges in the applied usage of the nanostructures as gas sensors is poor sensitivity. Nowadays, sensing properties of doped fullerenes, as a family of nanostructures, is one of the most interesting subjects [14, 31, 32]. Previous studies showed that doped fullerenes have strong affinity toward the small gases [31, 32]. The electronic and gas adsorption properties of graphene, CNT, BNNT, B_{12}, and C_{60} structures have been seriously affected by B and Al doping [18—23, 31, 33—35].

Various impurities in the petroleum industry and important atmospheric processes such as development of acid rain and ozone depletion are consist of sulfur-containing molecules [36, 37]. Several studies have focused on designing adsorbents for removing H_2S and SO_2 from gases [24, 25, 28, 29, 38—41].

In this study, we report the first-principles calculations on the interactions between H_2S and SO_2 with C_{20} fullerene. The sensitivity of the heterorfullerens toward the gases is analyzed.

COMPUTATIONAL DETAILS

DFT calculations were carried out using the GAMESS package [42] with B3LYP method at 6-31G++(*d*,*p*) basis set. Geometries of all the systems without any constraints were fully optimized. The compatibility of B3LYP with the fullerene-based nanostructures has been confirmed [43, 44]. Energy, natural population analysis (NPA) [45], and partial density of states (PDOS) of the optimized structures are also investigated to extract the conclusions on the stability, charge transfer (CT), and electronic structures. The corrected adsorption energy (E_{ads}) is given by:

$$E_{ads} = E_{cage\text{-}gas} - E_{cage} - E_{gas} + E_{BSSE}, \quad (1)$$

where $E_{cage\text{-}gas}$, E_{cage}, and E_{gas} are the energy of the gas on the cage, the fully relaxed cage, and the isolated gas molecule, respectively. Due to the unbalancing between the basis set used to describe the interacting system and the isolated reactants, E_{BSSE} is applied to correct the deviations of the adsorption energy [46]. According to Pearson, operational and approximate definitions of the electronic chemical potential (μ) and the absolute hardness (η) of a chemical system are given by [47]:

$$\mu \cong (-1/2)(IP + EA), \quad (2)$$

$$\eta = (1/2)(IP - EA), \quad (3)$$

where IP and EA are the ionization potential and electron affinity, respectively. According to Koopman′s theorem, the frontier orbital energies are given by [48]

$$IP = -E_{HOMO}, \quad (4)$$

$$EA = -E_{LUMO}. \quad (5)$$

Also, global softness (S) and electrophilicity index (ω) are computed from the orbital energies of the highest occupied molecular orbital (E_{HOMO}) and the lowest unoccupied molecular orbital (E_{LUMO}) at the same level of energy.

$$S = 1/2\eta, \quad (6)$$

$$\omega = \mu^2/2\eta. \quad (7)$$

The energy gap variation (ΔE_g) for any cage-gas complex is defined as

$$\Delta E_g = E_{g(cage\text{-}gas)} - E_{g(cage)}, \quad (8)$$

where E_g is differences between the highest occupied molecular orbital (HOMO) and the lowest unoccupied molecular orbital (LUMO). It should be noted that for systems with an odd number of total electrons, there are two distinct α and β E_g.

RESULTS AND DISCUSSION

The structural and electronic properties of C_{20}, BC_{19}, and AlC_{19}. First of all the C_{20} fullerene without any constraints has been optimized and shown in Fig. 1, *a*. The structural and electronic properties of the cages are listed in Tables 1 and 2. The average bond length, bond angle, and diameter of the C_{20} are about 1.44 Å, 108.72°, and 3.99 Å, respectively, which is in good agreement with the reported data [10, 12, 14, 16]. The cohesive energy (E_{coh}) as a good criterion for thermodynamic stability of the structure is calculated from the formula

$$E_{coh} = E_{cage} - n_C E_C - n_{Al} E_{Al} - n_B E_B, \quad (9)$$

where E_{cage} is the total energy of C_{20}, BC_{19} or AlC_{19}, and E_C, E_B, and E_{Al} are the energy of an isolated C, B, and Al atom, respectively, and n_c, n_B, and n_{Al} are the number of corresponding atoms. The total energy of the C_{20} is calculated to be –761.602 Hartree, in good agreement with previous QMC and

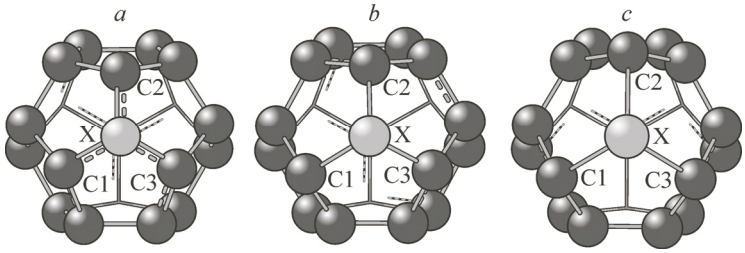

Fig. 1. The optimized structures of C_{20} (*a*), BC_{19} (*b*), and AlC_{19} (*c*)

DFT calculations [49, 50]. Larger absolute E_{coh} corresponds to more stability. Based on E_{coh}, C_{20} fullerene (E_{coh} = –7.84 eV/atom) is more reactive than both C_{60} (E_{coh} = –8.66 eV/atom) and AlC_{59} (–8.51 eV/atom) at the same level of theory. This is consistent with the previous studies [49—51]. Therefore, C_{20} is more useful than the C_{60} for further applications, and to calculate gas adsorption on the native and modified C_{20} fullerene can be of interest. The results show that H_2S and SO_2 molecules are adsorbed with E_{ads} of –0.04 and –0.2 eV, respectively. Furthermore, the minimum distance (R_{min}) between C_{20} and H_2S or SO_2 molecule are 3.9 and 2.52 Å, respectively. The adsorptions processes are exothermic, but the values of E_{ads} are not suitable for practical usage. One of the proposed methods to overcome the insensitivity is doping of the C_{20} by B or Al atoms. The dopant acts as an adsorption site for the gas molecules and induces CT between the cage and the adsorbed molecules, making the doped cage capable of sensing H_2S and SO_2. Fig. 1, *b*, *c* shows the fully relaxed geometries of the heterofullerenes. Important changes in the bond lengths, bond angles, and diameter near the heteroatom have been observed. The average bond lengths of B—C and Al—C are 1.56 Å and 1.93 Å, respectively. Moreover, average bond angles of C—B—C and C—Al—C are 106.97 and 93.26°, indicating sp^3 hybridization of the heteroatom. It is notable that, as revealed in Table 1, the cage diameter that passes through the heteroatom increases from 3.99 Å in the C_{20} to 4.23 Å and 4.76 Å in BC_{19} and AlC_{19}, respectively. Upon structural relaxation, the heteroatom is pushed outward from the surface and is ready to react with other molecules. So, protrusion of Al atom in AlC_{19} (0.77 Å) is larger than that of B atom in BC_{19} (0.24 Å), which can be described by atomic radius of heteroatom relative to that of the C atom [20, 52]. The protrusion of Al atom in CNT and C_{60} were calculated to be 0.812 and 0.76 Å, respectively [19]. The corresponding of the E_{coh} of BC_{19} and AlC_{19} are –7.75 and –7.55 eV/atom, respec-

T a b l e 1

Structural parameters of C_{20}, BC_{19}, *and* AlC_{19} *cages*

System	Bond length, Å			Bond angle, deg.			Diameter, Å	Protrusion, Å
	C1—X	C2—X	C3—X	C1—X—C2	C1—X—C3	C2—X—C3		
C_{20}	1.44	1.44	1.44	108.73	108.73	108.71	3.99	—
BC_{19}	1.56	1.56	1.56	108.21	108.16	104.55	4.23	0.24
AlC_{19}	1.93	1.93	1.94	94.80	90.25	94.73	4.76	0.77

T a b l e 2

Cohesive energy (E_{coh}), *band gap* (E_g), *ionization potential* (*IP*), *electrophilicity index* (ω), *chemical potential* (μ), *hardness* (η), *softness* (S) *and dipole moment* (μ_D) *of* C_{20}, BC_{19}, *and* AlC_{19} *cages*. α *and* β *denote spin up and down, respectively*

System	E_{coh}, eV/atom	E_g, eV	*IP*, eV	ω, eV	μ, eV	η, eV	S, eV	μ_D, D
C_{20}	–7.84	1.91	5.536	10.03	–4.580	0.956	0.523	0.00
BC_{19}	–7.74	1.86^{α}, 3.15^{β}	5.478	9.615	–4.548	0.930	0.538	0.27
AlC_{19}	–7.55	1.60^{α}, 2.7^{β}	5.248	7.908	–4.448	0.800	0.626	4.08

Table 3

Natural population analysis (NPA) *and natural atomic orbital occupancies of heteroatoms in free and in the cage*

System	NPA	2*s*	2p_x	2p_y	2p_z	3*s*	3p_x	3p_y	3p_z
B	0.00	2.00	1.00	0.00	0.00	0.00	0.00	0.00	0.00
BC_{19}	+0.71	0.64	0.46	0.55	0.64	0.00	0.00	0.00	0.00
Al	0.00	2.00	2.00	2.00	2.00	2.00	1.00	0.00	0.00
AlC_{19}	+1.63	2.00	2.00	2.00	2.00	0.68	0.14	0.28	0.26

tively. Thus, AlC_{19} must be more reactive than BC_{19} and C_{20} structures. The same trend was also observed for AlC_{59}, BC_{59}, and C_{60} fullerenes [53].

NPA and natural atomic orbital occupancies of the heteroatoms are summarized in Table 3. After dopage the B atom loses 1.36 |e| and gains 0.63 |e| in 2*s* and 2*p* orbitals, respectively. Therefore, both donation and back-donation of electron density occurs. On the other hand, the Al atom loses 1.32 |e| and 0.32 |e| of its charge from 3*s* and 3*p* orbitals, respectively. This finding shows that the 3*s* orbital has a stronger interaction with the neighboring atoms than the 3*p* orbital. In both cases, the p_x orbital loses electron density, whereas the p_y and p_z orbitals get more of it. As it can be seen from Table 3, there is an obvious electron deficient region on the B and Al atoms, consistent with a considerable positive electrostatic charge +0.71 |e| and +1.63 |e| for B and Al atoms, respectively. This suggests that the doping with Al and B atom forms electronic holes in the fullerene cage.

Chemical reaction for the reactant molecules can also be explained based on frontier molecular orbitals (FMO). PDOS of the C_{20}, BC_{19}, and AlC_{19} are depicted in Fig. 2. Calculated E_g of the cages are listed in Table 2. E_g for C_{20} is 1.91 eV. Many different results were reported for E_g of C_{20} [6, 7, 12, 16, 17]. These deviations can be attributed to the choice of the functional and variety of methods. PBE and B3LYP functional give different results, and the results from PBE are generally underestimated [17]. The geometrical changes would result in different electronic properties of the cages. Electronic structure analysis demonstrated that energy of HOMO level is more sensitive than LUMO level to the doping. In both BC_{19} and AlC_{19}, the HOMO levels shift towards more stable states, but this change is not visualized for the LUMO levels. As a result of removing peak in –5.6 eV, E_g for the β level of BC_{19} and AlC_{19} are changed to 3.15 and 2.7 eV, respectively. Notably that the α gap of BC_{19} and AlC_{19} is smaller than β one. Therefore, the electronic properties of the systems are determined by the α level. The electrical conductivity of C_{20} should be increased upon B- and Al-doping, which is consistent with the NPA results. Abundance of fullerene structures is related to both thermodynamic and kinetic stability. Since electron transition from HOMO to LUMO is energetically inappropriate, the structures with larger E_g have higher kinetic stability and low reactivity [54]. Thus the kinetic stability of the cage is decreased upon substitution. Therefore, the doped cage with smaller heteroatom is more stable. The same trends for η, ω, E_{coh}, and E_g have also been observed. As listed in Table 2, BC_{19} and AlC_{19} have smaller IP, which confirms that the new cages can easily lose electrons. The tendency of a system to obtain additional charge and a measure of the electrophilic power of a molecule is described by the quantity of ω (Table 2). When two molecules react with each other, one of them acts as nucleophile while the other one acts as electrophile. There is a direct relationship between ω and electrophilic nature of a molecule. Based on ω, AlC_{19} loses more electrons than BC_{19} and C_{20}. Thus, AlC_{19} and BC_{19} act as nucleophilic species. Increasing in η, which is like a stamina toward the deformation in the presence of an electric field, leads to an increase in the stability, and reduces the reactivity of the chemical species [55]. The S parameter is another index which has an inverse relationship with η. Therefore, AlC_{19} has a maximum instability and reactivity respect to the other cages. From the above discussion, the reactivity trend is $AlC_{19} > BC_{19} > C_{20}$.

The B and Al elements are the active site and the sensing element of the modified cages. In continuation of the work, the structures and energies of minimum adsorption configurations of H_2S and SO_2 molecules with various possible initial adsorption geometries were investigated. For each adsor-

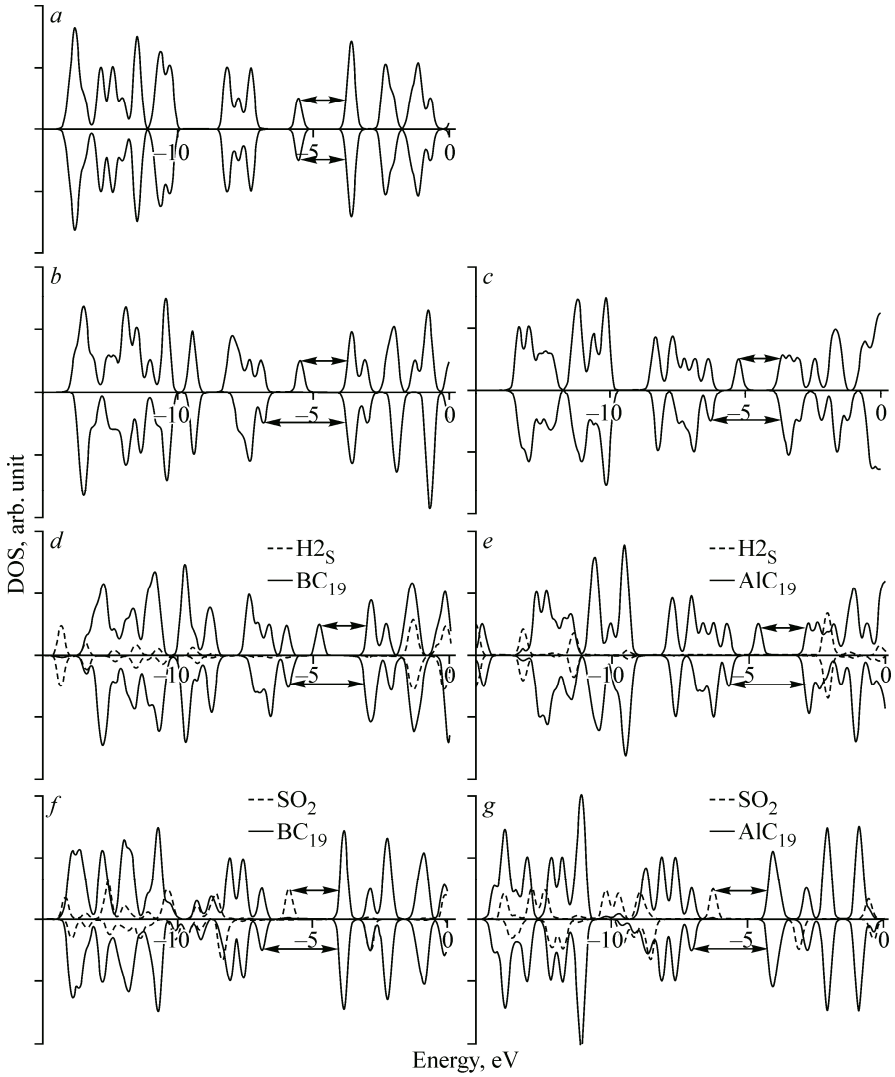

Fig. 2. Partial density of states for C_{20} (*a*), BC_{19} (*b*), AlC_{19} (*c*), $H_2S@BC_{19}$ (*d*), $H_2S@AlC_{19}$ (*e*), $SO_2@BC_{19}$ (*f*), and $SO_2@AlC_{19}$ (*g*).
The upper and lower panels are PDOS for spin up and spin down, respectively. The band gaps are shown by the arrows

bate, two adsorption sites, namely, on the top of a heteroatom and the center of pentagon with an impurity atom, with different configurations are evaluated.

H_2S on fullerenes. The most stable configurations of H_2S adsorbed on the heterofullerens are shown in Fig. 3, *a*, *c*. Tables 4—6 summarize the calculated structural and electronic parameters for the most optimized configuration of cage-H_2S complex. In these configurations, R_{min} between B and Al atoms and the S atom are 2.05 and 2.48 Å, respectively. CT pathway can be explained by interactions between the HOMO of one species and the LUMO of the other one. As can be seen from Table 5, |LUMO(H_2S)—HOMO(cage)| is larger than |LUMO(cage)—HOMO(H_2S)|. Thus, the electrons transfer from H_2S to cages is due to a small energy barrier. This interpretation is consistent with the findings from NPA. According to the NPA (Table 4), the H_2S molecule loses 0.53 |e| and 0.32 |e| on BC_{19} and AlC_{19}, respectively. The positive sign indicates the electron transfer from H_2S to the cages. The same behavior is observed between H_2S and the other adsorbents [24, 28—30]. The S—H bond lengths increase from 1.348 Å in isolated H_2S to 1.352 Å and 1.353 Å for S—H1 and S—H2 bonds on both heterofullerens (Table 6). As a result of CT from bonding orbital, the elongation of the bond lengths is justified. In addition, the H—S—H bond angle is increased from 92.472° to 93.386 and

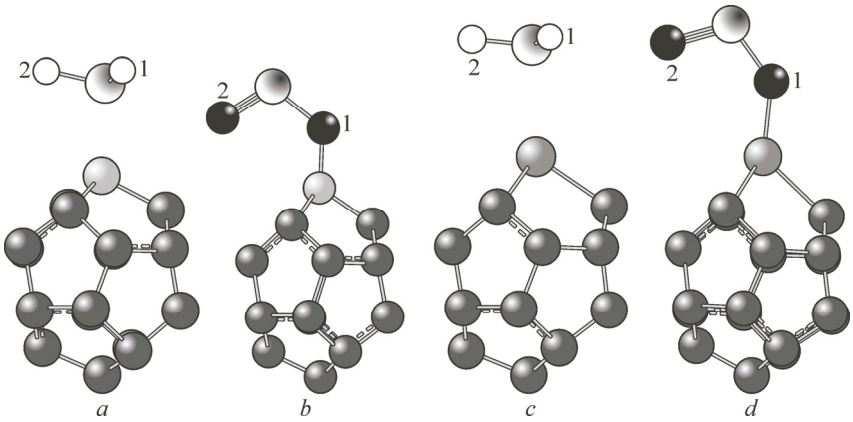

Fig. 3. The optimized structures of $H_2S@BC_{19}$ (*a*), $SO_2@BC_{19}$ (*b*), $H_2S@AlC_{19}$ (*c*), $SO_2@AlC_{19}$ (*d*)

T a b l e 4

Structural and electronic properties of the most stable form of gas-cage system. Including minimum distance of cage-gas (R_{min}), *amount of difference of protrusion before and after gas adsorption* (ΔP) ($\Delta P = P_{after} - P_{before}$), *band gap* ($E_g$), *the amount of difference of* E_g *before and after adsorption* (ΔE_g), *amount of* CT *from gas to cage* (Q_T), *amount of charge on* B *or* Al *atom in the complexes from* NPA (Q_X) (X = B *or* Al)), *dipole moment* (μ_D), *and corrected adsorption energy* (E_{ads})

System	R_{min}, Å	ΔP, Å	E, eV	ΔE_g, eV	Q_T, |e|	Q_X, |e|	μ_D, D	E_{ads}, eV
BC_{19}—H_2S	2.05	0.2	1.85^{α}, 2.90^{β}	-0.01^{α}, -0.25^{β}	+0.53	0.33	6.93	–0.43
BC_{19}—SO_2	1.44	0.39	2.00^{α}, 3.02^{β}	$+0.14^{\alpha}$, -0.13^{β}	–0.49	0.63	2.75	–1.7
AlC_{19}—H_2S	2.48	0.07	1.84^{α}, 2.87^{β}	$+0.24^{\alpha}$, $+0.17^{\beta}$	+0.32	1.41	10.18	–0.91
AlC_{19}—SO_2	1.75	0.3	2.21^{α}, 3.03^{β}	$+0.61^{\alpha}$, $+0.33^{\beta}$	–0.69	1.75	2.62	–3.03

T a b l e 5

Electrical structure parameters of the adsorption structures

Molecule	E(HOMO)	E(LUMO)	$\|E_{LUMO}$(cage)—E_{HOMO}(gas)|	$\|E_{LUMO}$(gas)—E_{HOMO}(cage)|
BC_{19}	–5.48	–3.62		
H_2S	–7.30	–0.26	3.68	5.22
SO_2	–9.46	–4.11	5.84	1.37
AlC_{19}	–5.25	–3.65		
H_2S	–7.30	–0.26	3.65	4.99
SO_2	–9.46	–4.11	5.75	1.14

T a b l e 6

Structural parameters of gas-cage complexes. X *is denoted* B *or* Al *atoms*

System	Bond length, Å							Bond angle, deg.	
	C1—X	C2—X	C3—X	H1—S	H2—S	O1—S	O2—S	H1—S—H2	O1—S—O2
BC_{19}—H_2S	1.615	1.622	1.617	1.352	1.353			93.386	
AlC_{19}—H_2S	1.950	1.948	1.945	1.353	1.353			93.551	
BC_{19}—SO_2	1.668	1.670	1.654			1.501	1.648		111.073
AlC_{19}—SO_2	2.009	2.011	2.010			1.500	1.629		109.653

93.551° on BC_{19} and AlC_{19}, respectively. This increase can be attributed to the hindrance effect. The average C—X bond lengths in the heteropentagon ring increases from 1.56 Å to 1.62 Å and from 1.93 Å to 1.95 Å for BC_{19} and AlC_{19}, respectively. Large changes in BC_{19} are consistent with more CT toward BC_{19}. The charge on B and Al atoms are 0.33 and 1.41 |e|, respectively. The E_{ads} of H_2S on BC_{19} and AlC_{19} are –0.43 and –0.91 eV, respectively. The adsorptios of H_2S on the heterofullerenes is more exothermic than that on the fullerene. From the above analysis, the H_2S interaction with the BC_{19} is stronger than with C_{20}, and the strongest interaction is with AlC_{19}. Furthermore, the H_2S interaction with AlC_{19} is stronger than with CNT [30], AlN nanotube [24], Fe(110) [56], Pd(111) [39], BC_3 sheet [57], but weaker than with Au-doped CNT [28] and Si-doped CNT [30]. Therefore, H_2S can be effectively adsorbed on the surface of both BC_{19} and AlC_{19}. Hence, both cages can be used for adsorption.

To elucidate further the adsorption processes of H_2S, the PDOSs plots of the cages and H_2S are shown in Fig. 2, *d*, *e*. Although a medium hybridization between the gas and cages in the region of –14 to –9 eV and –3 to 0 eV occurs; the H_2S adsorption has no sensible effects on the electronic properties of BC_{19}, whereas the gap of the α level on AlC_{19} increases by about 0.24 eV. Therefore, the AlC_{19} conductivity decreases. As a result, BC_{19} cannot be a good sensor for H_2S gas, whereas AlC_{19} can.

SO_2 on fullerenes. After careful structural optimizations without any constraints, it is found that one of the oxygen atoms (O1) in SO_2 is bonded to the heteroatom (Fig. 3, *b* and *d*). The structural and electronic properties of the most stable adduct in the cage-SO_2 system are summarized in Tables 4—6. In this configuration, R_{min} between B and Al atoms to O1 of SO_2 are 1.44 Å and 1.75 Å, respectively. The |LUMO(SO_2)—HOMO(cage)| is smaller than |LUMO(cage)—HOMO(SO_2)| (Table 5). The electron needs to cross an energy barrier of more than 5.7 eV to be transferred from SO_2 to the cages. The NPA results are confirmed by this interpretation. The NPA shows that the SO_2 molecule withdraw about 0.49 and 0.69 |e| charge from BC_{19} and AlC_{19}, respectively, owing to higher electronegativity of the O atoms. The same behavior is also observed with other adsorbents [25—28, 40, 58]. Because of the strong adsorption of SO_2, CT is remarkable. Influence of Al doping can be confirmed by large CT from AlC_{19} to SO_2 gas (Table 4). Meanwhile, the electrons fill the antibonding orbital of SO_2. Thus, bond lengths increase from 1.46 Å in isolated SO_2 to 1.50 Å and 1.65 Å for S—O1 and S—O2 bonds in the BC_{19}—SO_2, and to 1.50 Å and 1.63 Å in the AlC_{19}—SO_2 system. The O—S—O angle decreases from 118.7° to 111.1° and 109.6° for BC_{19} and AlC_{19}, respectively. The significant structural changes in the heterofullerenes are explained by the strong attraction of SO_2. As a result of the C—X bond length elongation (Table 6), the bond energy and bond activity are decreased and increased, respectively. The B—C1, B—C2, B—C3 Al—C1, Al—C2, and Al—C3 bonds are elongated by 6.9, 7, 6.8, 4, 4.2, and 4.1 %, respectively. The SO_2 molecule is adsorbed with the binding energy of –1.7 and –3.03 eV on BC_{19} and AlC_{19}, respectively. Sensing of the gases requires relatively strong interactions between gas molecules and a sensor. The strong interaction of SO_2 on AlC_{19} is not favorable for a gas sensor, but BC_{19} can be a good sensor for SO_2. E_{ads} on AlC_{19} is larger than that on B- and Al-doped graphene [22], Au-doped CNT [28], Pd-doped CNT [27], Ni-doped CNT [59], GeC nanotube [40], AlN nanotube and nanosheet [25, 58], and $Zn_{12}O_{12}$ nanocage [26].

The PDOS plots are shown in Fig. 2. Upon adsorption of the SO_2 molecule, great changes in PDOS happen. The HOMO and LUMO levels of the cages shift to lower energy states, while opposite shifting is evidenced for H_2S adsorption. After SO_2 adsorption, the HOMO and LUMO of the α level are exclusively constituted by the SO_2 (100 %) and cage MO (100 %), respectively. The states of SO_2 and cages overlap in the energy region of –14 to –7 eV. An impurity peak can be seen in the region of –5.9 and –6.34 eV for BC_{19}—SO_2 and AlC_{19}—SO_2 adducts. The E_g values of BC_{19}—SO_2 and AlC_{19}—SO_2 are larger by 0.14 and 0.61 eV than those of free BC_{19} and AlC_{19}. This suggests that the cage-SO_2 adduct remains semiconductor in nature. Electron hopping over a large HOMO and LUMO gap is difficult and thus could diminish the conductance of the sensors. In conclusion, BC_{19} and AlC_{19} have a good sensitivity to SO_2 and can be used to detect SO_2 gas based on the changes in its conductivity. Hence, we propose that both BC_{19} and AlC_{19} may be suitable for detecting the presence of SO_2 molecules.

Electric dipole moment and vibrational frequencies. The charge distribution in the structures is shown by electric μ_D in Tables 2 and 4. Upon dopage, μ_D of the heterofullerens are increased. The structure with a large protrusion showed large μ_D. The μ_D values for BC_{19} and AlC_{19} are 0.27 and 4.08 D, respectively. For the H_2S adducts with BC_{19} and AlC_{19} these values are 6.93 and 10.18 D, respectively. The sizes of the μ_D vector of the cages are changed and increased by adsorption of the H_2S molecule. Interestingly, the SO_2 gas molecule has different behavior on total μ_D of the heterofullerenes. The size and direction of the electric μ_D vector is changed. Upon SO_2 adsorption, μ_D of the BC_{19} and AlC_{19} adducts as a criterion of charge distribution is increased and decreased, respectively. This contradiction is related to the polarization turning. It seems that there is a direct relationship between μ_D of free molecules and E_{ads}. SO_2 and AlC_{19} molecules with larger μ_D values (2.01 and 4.08 D) have the largest amounts of E_{ads}, whereas H_2S and BC_{19} molecules with lower μ_D (1.30 and 0.27 D, respectively) have smaller amounts of E_{ads}. The complexes with large μ_D may have potential applications in dielectrics and solid state materials.

Local minima on the potential energy surface of the cages with and without the gases are confirmed by the vibrational frequency analysis. The calculated vibrational frequencies for all the cages show no imaginary vibrational frequency, indicating that the structures correspond to the true minima. The calculated infrared (IR) spectra are plotted in Fig. 4. The C_{20} molecule has 54 frequency modes totally. From Fig. 4 we can see that C_{20} has two distinct peaks at 730 and 1350 cm^{-1}. As for the doped cages, their IR spectra are more complicated. The original two peaks are split and additional absorption is present. These absorptions all exhibit a red or blue shift as compared with those of the pristine cage. Furthermore, it can be seen that there are also several new peaks in the range of 250—500 cm^{-1} for AlC_{19}, while there are no such peaks for C_{20} and BC_{19}. As shown in Fig. 4, *d*, *e*, a sharp peak is observed at 686 and 404 cm^{-1} for BC_{19}—H_2S and AlC_{19}—H_2S adducts, respectively. A small peak around 2650 cm^{-1} for both heterofullerene adducts with H_2S appears. Two strong peaks at 1040 and 1130 cm^{-1} for BC_{19}—SO_2, and a distinct peak around 930 cm^{-1} for AlC_{19}—SO_2 can be used as finger

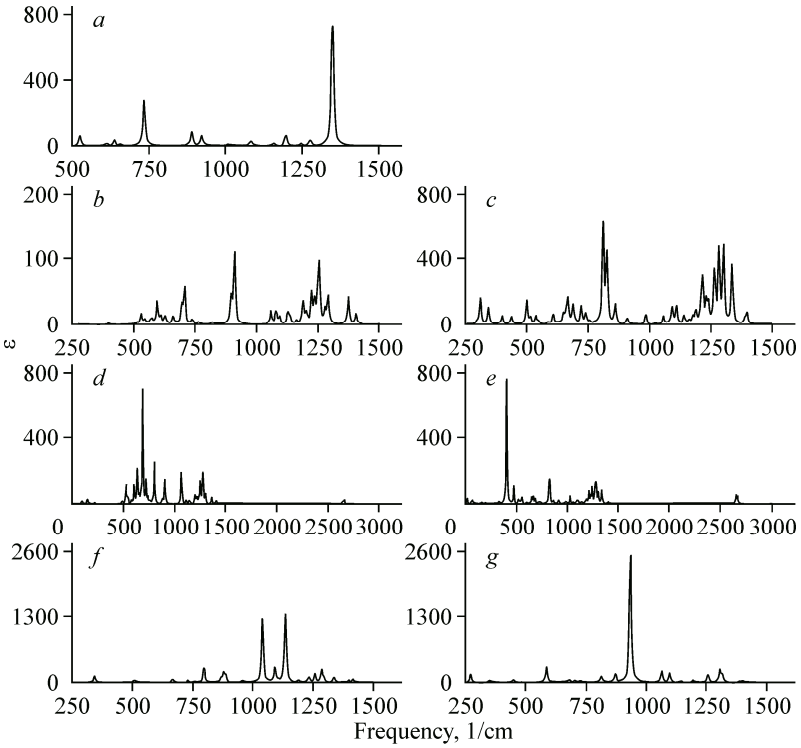

Fig. 4. The calculated IR spectra of the C_{20} (*a*), BC_{19} (*b*), AlC_{19} (*c*), $H_2S@BC_{19}$ (*d*), $H_2S@AlC_{19}$ (*e*), $SO_2@BC_{19}$ (*f*), and $SO_2@AlC_{19}$ (*g*)

prints (Fig. 4, *f* and *g*). It can be seen that the shapes of IR absorption spectra are different for the different doped cages. These characteristic features in the IR spectra could be helpful to identify these heterofullerenes with and without gas molecules from the experimental spectra.

CONCLUSIONS

DFT calculations were performed to study H_2S and SO_2 gas adsorption on the BC_{19} and AlC_{19} heterofullerenes. After doping C_{20} with B or Al, the local structure around the impurity region is affected. Furthermore, the C_{20} conductivity was increased by doping. According to the calculated cohesive energies, the heterofulleren with a smaller heteroatom is more stable. The results show that BC_{19} is not a good sensor for detecting H_2S, while the electronic structure of AlC_{19} is much affected by H_2S adsorption. Both heterofullerens are suitable sensors for SO_2. Moreover, SO_2 has a profound impact on the electronic structure of the heterofullerens and decreases their electrical conductivity. The C_{20} reactivity toward H_2S and SO_2 would be improved by doping with B and Al atoms. The IR absorptions exhibit red or blue shifts after the introduction of heteroatoms as compared with IR of pristine C_{20}. We believe that the present work may help to develop new fullerene-based systems for gas sorption and sensing.

REFERENCES

1. *Richeson D.S.* Euler′s Gem: The polyhedron formula and the birth of topology. – Princeton University Press, 2012.
2. *Smalley R.E., Kroto H., Heath J.* // Nature. – 1985. – **318**. – P. 162 – 163.
3. *Prinzbach H., Weiler A., Landenberger P., Wahl F., Wörth J., Scott L.T., Gelmont M., Olevano D., Issendorff B.v.* // Nature. – 2000. – **407**. – P. 60 – 63.
4. *Wang Z., Ke X., Zhu Z., Zhu F., Ruan M., Chen H., Huang R., Zheng L.* // Phys. Lett. A. – 2001. – **280**. – P. 351 – 356.
5. *Iqbal Z., Zhang Y., Grebel H., Vijayalakshmi S., Lahamer A., Benedek G., Bernasconi M., Cariboni J., Spagnolatti I., Sharma R.* // // Europ. Phys. J. B. – Condensed Matter and Complex Systems. – 2003. – **31**. – P. 509 – 515.
6. *Sawtarie M., Menon M., Subbaswamy K.* // Phys. Rev. B. – 1994. – **49**. – P. 7739.
7. *An Y.-P., Yang C.-L., Wang M.-S., Ma X.-G., Wang D.-H.* // J. Cluster Sci. – 2011. – **22**. – P. 31 – 39.
8. *An Y.-P., Yang C.-L., Wang M.-S., Ma X.-G., Wang D.-H.* // J. Chem. Phys. – 2009. – **131**. – P. 24311.
9. *Saito M., Miyamoto Y.* // Phys. Rev. B. – 2002. – **65**. – P. 165434.
10. *Davydov I., Podlivaev A., Openov L.* // Phys. Solid State. – 2005. – **47**. – P. 778 – 784.
11. *Saito M., Miyamoto Y.* // Phys. Rev. Lett. – 2001. – **87**. – P. 035503.
12. *Kumar R., Rani A.* // Phys. B: Condens. Matter. – 2011. – **406**. – P. 1173 – 1177.
13. *Sackers E., Oßwald T., Weber K., Keller M., Hunkler D., Wörth J., Knothe L., Prinzbach H.* // Chem. Europ. J. – 2006. – **12**. – P. 6242 – 6254.
14. *Kassaee M., Buazar F., Koohi M.* // J. Mol. Struct.: THEOCHEM. – 2010. – **940**. – P. 19 – 28.
15. *Chen Z., Heine T., Jiao H., Hirsch A., Thiel W., Schleyer P.v.R.* // Chem. Europ. J. – 2004. – **10**. – P. 963 – 970.
16. *Baei M.T.* // Heteroatom. Chem. – 2013. – **24**. – P. 516 – 523.
17. *Ghiasi R., Fashami M.Z., Hakimioun A.H.* // Theor. Comput. Chem. – 2014. – **13**. – P. 1450023.
18. *Ao Z., Jiang Q., Zhang R., Tan T., Li S.* // J. Appl. Phys. – 2009. – **105**. – P. 074307.
19. *Azizi K., Karimpanah M.* // Appl. Surf. Sci. – 2013. – **285**. – P. 102 – 109.
20. *Wang R., Zhang D., Sun W., Han Z., Liu C.* // J. Mol. Struct.: THEOCHEM. – 2007. – **806**. – P. 93 – 97.
21. *Ao Z., Yang J., Li S., Jiang Q.* // Chem. Phys. Lett. – 2008. – **461**. – P. 276 – 279.
22. *Dai J., Yuan J., Giannozzi P.* // Appl. Phys. Lett. – 2009. – **95**. – P. 232103 – 232105.
23. *Bai L., Zhou Z.* // Carbon. – 2007. – **45**. – P. 2105 – 2110.
24. *Beheshtian J., Ahmadi Peyghan A., Bagheri Z.* // Phys. E: Low-dimensional Systems and Nanostructures. – 2012. – **44**. – P. 1963 – 1968.
25. *Beheshtian J., Baei M.T., Peyghan A.A., Bagheri Z.* // J. Mol. Modeling. – 2012. – **18**. – P. 4745 – 4750.
26. *Baei M.T., Tabar M.B., Hashemian S.* // Adsorption Science & Technology. – 2013. – **31**. – P. 469 – 476.
27. *Zhou X., Tian W.Q., Wang X.-L.* // Sensors and Actuators B: Chemical. – 2010. – **151**. – P. 56 – 64.
28. *Zhang X., Dai Z., Chen Q., Tang J.* // Physica Scripta. – 2014. – **89**. – P. 065803.
29. *Peyghan A.A., Soleymanabadi H.* // Mol. Phys. – 2014. – **112**. – P. 2737 – 2745.
30. *Guo G., Wang F., Sun H., Zhang D.* // Internat. J. Quant. Chem. – 2008. – **108**. – P. 203 – 209.

31. *Grynko D., Burlachenko J., Kukla O., Kruglenko I., Belyaev O.* // Semiconductor Phys., Quantum Electronics & Optoelectronics. – 2009. – **12**. – P. 287 – 289.
32. *Tian C., Wang Z., Jin M., Zhao W., Meng Y., Wang F., Feng W., Liu H., Ding D., Wu D.* // Chem. Phys. Lett. – 2011. – **511**. – P. 393 – 398.
33. *Azizi K., Salabat K., Seif A.* // Appl. Surface Sci. – 2014. – **309**. – P. 54 – 61.
34. *Böyükata M., Güvenç Z.B.* // J. Hydrogen Energy. – 2011. – **36**. – P. 8392 – 8402.
35. *Zhang Y., Zhang Y., Zhang D., Liu C.* // J. Phys. Chem. B. – 2006. – **110**. – P. 4671 – 4674.
36. *Change I.P.o.C., Metz B., Kuijpers L., Solomon S., Anderson S.O., Davidson O.R., Pons J., De Jager D., Kestin T., Manning M.* Safeguarding the ozone layer and the global climate system: issues related to hydrofluorocarbons and perfluorocarbons, 2013.
37. *Speight J.G.* The chemistry and technology of petroleum. – CRC press, 2014.
38. *Jia Y., Zhuang G., Wang J.* // J. Phys. D: Appl. Phys. – 2012. – **45**. – P. 065305.
39. *Hyman M.P., Loveless B.T., Medlin J.W.* // Surface Sci. – 2007. – **601**. – P. 5382 – 5393.
40. *Samanta P.N., Das K.K.* // Chem. Phys. Lett. – 2013. – **577**. – P. 107 – 113.
41. *Guo Y., Li Y., Zhu T., Ye M., Wang X.* // Adsorption. – 2013. – **19**. – P. 1109 – 1116.
42. *Schmidt M.W., Baldridge K.K., Boatz J.A., Elbert S.T., Gordon M.S., Jensen J.H., Koseki S., Matsunaga N., Nguyen K.A., Su S.* // J. Comput. Chem. – 1993. – **14**. – P. 1347 – 1363.
43. *Saha D., Deng S.* // Langmuir. – 2011. – **27**. – P. 6780 – 6786.
44. *Wang D.-L., Xu H.-L., Su Z.-M., Hou D.-Y.* // Comput. Theor. Chem. – 2011. – **978**. – P. 166 – 171.
45. *Akdim B., Kar T., Duan X., Pachter R.* // Chem. Phys. Lett. – 2007. – **445**. – P. 281 – 287.
46. *Boys S.F., Bernardi F.d.* // Mol. Phys. – 1970. – **19**. – P. 553 – 566.
47. *Pearson R.G.* // Inorg. Chem. – 1988. – **27**. – P. 734 – 740.
48. *Koopmans T.* // Physica. – 1933. – **1**. – P. 104 – 113.
49. *Sokolova S., Lüchow A., Anderson J.B.* // Chem. Phys. Lett. – 2000. – **323**. – P. 229 – 233.
50. *Wang Z., Day P., Pachter R.* // Chem. Phys. Lett. – 1996. – **248**. – P. 121 – 126.
51. *Grossman J.C., Mitas L., Raghavachari K.* // Phys. Rev. Lett. – 1995. – **75**. – P. 3870.
52. *Yeung C.S., Liu L.V., Wang Y.A.* // J. Phys. Chem. C. – 2008. – **112**. – P. 7401 – 7411.
53. *Bai H., Ji W., Liu X., Wang L., Yuan N., Ji Y.* // J. Chem. – 2013. – **2013**. – P. 571709.
54. *Aihara J.-i.* // Theor. Chem. Acc. – 1999. – **102**. – P. 134 – 138.
55. *Gao B., Zhao J.-x., Cai Q.-h., Wang X.-g., Wang X.-z.* // J. Phys. Chem. A. – 2011. – **115**. – P. 9969 – 9976.
56. *Jiang D., Carter E.A.* // Surface Sci. – 2005. – **583**. – P. 60 – 68.
57. *Peyghan A.A., Soleymanabadi H.* // Mol. Phys. – 2014. – **112**. – P. 2737 – 2745.
58. *Rastegar S.F., Hadipour N.L., Soleymanabadi H.* // J. Mol. Modeling. – 2014. – **20**. – P. 1 – 6.
59. *Li W., Ma J.-J., Liu P., Pan Z.-L., He Q.-Y.* // Appl. Surface Sci. – 2015. – **335**. – P. 17 – 22.